Hostettler, Roland; Särkkä, Simo

IMU and magnetometer modeling for smartphone-based PDR

Published in:
2016 International Conference on Indoor Positioning and Indoor Navigation, IPIN 2016

DOI:
10.1109/IPIN.2016.7743695

Published: 14/11/2016

Document Version
Peer-reviewed accepted author manuscript, also known as Final accepted manuscript or Post-print

Please cite the original version:
Hostettler, R., & Särkkä, S. (2016). IMU and magnetometer modeling for smartphone-based PDR. In *2016 International Conference on Indoor Positioning and Indoor Navigation, IPIN 2016* Article 7743695 (International Conference on Indoor Positioning and Indoor Navigation). IEEE. https://doi.org/10.1109/IPIN.2016.7743695

IMU and Magnetometer Modeling for Smartphone-based PDR

Roland Hostettler and Simo Särkkä

DOI

10.1109/IPIN.2016.7743695

IMU and Magnetometer Modeling for Smartphone-based PDR

Roland Hostettler and Simo Särkkä

Department of Electrical Engineering and Automation
Aalto University, Espoo, Finland
Email: { roland.hostettler, simo.sarkka }@aalto.fi

***Abstract*—In this paper, IMU and magnetometer models that enable pedestrian dead-reckoning without step detection or zero velocity updates on hand-held devices such as smartphones are proposed. The models are suitable for usage with any standard Bayesian filtering or smoothing technique and thus, do not require customized estimators. The method is evaluated in a real scenario using a dataset of approximately three minutes with a trajectory length of $302\,\mathrm{m}$. It is found that the overall shape of the estimated trajectory matches well with the GPS reference trajectory with an estimated trajectory length of $293\,\mathrm{m}$. Some problems in the heading estimation are observed.**

I. Introduction

Pedestrian dead reckoning (PDR) has become a promising low-cost method for a wide range of applications such as tracking and navigating for first responders at accident sites [1] or more consumer-oriented applications such as navigation in areas with limited coverage of global navigation satellite systems. The advance of PDR is largely due to the increasing availability of low-cost microelectromechanical systems-based inertial measurement units (IMUs) and magnetometers in smartphones, wearables, or specifically designed sensor platforms.

Compared to traditional strap-down navigation [2] where the IMU is affixed to the moving platform and motion is relatively smooth, the sensors can generally move more freely and are subject to much more variable movements in PDR. A notable exception to this is foot-mounted PDR [3], [4] where dedicated sensors are mounted to a user's leg or embedded into their shoe. Such solutions work well for professional personnel such as firefighters or first responders where an additional device can be seen as part of their equipment. Thus, it has gained considerable attention and well working solutions, mostly based on an error-formulation Kalman filter with filter updates during the stationary phase (zero velocity and/or zero angular rate updates) have been developed [5], [6]. However, these solutions are limitedly useful for consumer applications as the users might be reluctant to wearing extra sensors mounted to their legs just for navigating. Instead, it is desirable to make good use of the existing sensors in smartphones, activity trackers, and smartwatches. Since techniques such as zero-velocity updates can not be used reliably for hand-held (or pocket-carried) devices, other approaches suitable for this problem are required.

978-1-5090-2425-4/16/$31.00

Existing solutions for such problems are often based on a combination of step detection together with step length estimation and subsequent integration [6], [7]. For example, in [8], step detection and heading estimation algorithms are developed and combined with existing step length models to build a PDR system. A more advanced solution that takes different user behavior and device carrying situations into account is developed in [9]. Furthermore, simple filtering- and integration algorithms have been considered in [10] for different measurement setups. A step back from the more and more fine-grained approaches that rely on motion mode detection, a simplified and more robust method relying on sensor orientation tracking, robust step detection with step validation, and heading estimation is proposed and evaluated in [11].

In contrast to these existing methods, the contributions of this paper are as follows. First, complete sensor models linking the phenomena observed by the accelerometer, gyroscope, and magnetometer to the dynamic motion of the user are proposed. The developed models are suitable for using in sequential Bayesian filtering and smoothing techniques such as Kalman filters. This provides a different approach to PDR, eliminating the need for step detection and integration. The proposed approach is then evaluated using real experiments with a commercially available device.

The remainder of this paper is organized as follows. The dynamic models and measurement models are developed in Section II. Estimation using the developed models is presented in Section III, followed by the experimental evaluation and discussion presented in Section IV. Some concluding remarks are given in Section V.

II. Model

In this section, the dynamic model describing the (constrained) motion of the pedestrian and the proposed observation model relating the IMU measurements to the dynamic model are developed.

A. Dynamic Model

In the vast majority of the literature, the pedestrian motion is modeled using a constant velocity motion model in the global coordinate system. However, since the motion of the pedestrian is in most cases in the forward direction as seen

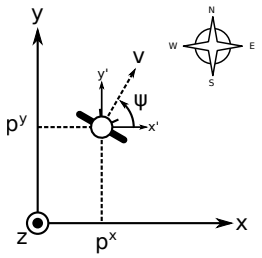

Fig. 1. Illustration of the coordinate system. The global coordinate system is translated to the coordinate system x′-y′ by the person's location p_t^{G} and then rotated about the heading ψ_t to yield the person's local coordinate system.

from the pedestrian, the proposed model is parametrized as a constant turn motion model in the x-y-plane with speed v_t in the walking direction and rotation (yaw ψ_t) around the persons vertical axis, that is, in the person's local coordinate frame[1] (see Fig. 1). The dynamic equations for the person are then given by

$$\frac{\mathrm{d}p_t^{\mathsf{G}}}{\mathrm{d}t} = v_t^{\mathsf{G}}, \tag{1a}$$
$$\frac{\mathrm{d}v_t}{\mathrm{d}t} = \eta_{v,t}, \tag{1b}$$
$$\frac{\mathrm{d}\psi_t}{\mathrm{d}t} = \omega_t, \tag{1c}$$
$$\frac{\mathrm{d}\omega_t}{\mathrm{d}t} = \eta_{\omega,t}, \tag{1d}$$

where the superscript G indicates the global East-North-Up (ENU) coordinate frame, and the subscript t denotes continuous time. $p_t^{\mathsf{G}} \in \mathbb{R}^2$ is the position in the x-y-plane, $v_t \in \mathbb{R}$ the speed which is modeled as a random walk process with $\eta_{v,t}$ being a zero-mean white noise process with covariance S_v. Furthermore, $\psi_t \in \mathbb{R}$ is the heading and $\omega_t \in \mathbb{R}$ denotes the yaw velocity, also modeled as a zero-mean white noise process $\eta_{\omega,t}$ with covariance S_ω. The global velocity vector $v_t^{\mathsf{G}} \in \mathbb{R}^2$ is given by

$$v_t^{\mathsf{G}} = v_t \begin{bmatrix} \cos(\psi_t) \\ \sin(\psi_t) \end{bmatrix}. \tag{2}$$

Since the IMU is not assumed to be firmly affixed to the person's body, it can move freely. While the translation relative to the person is small (in the range of $< 0.5\,\mathrm{m}$) and is assumed negligible, the attitude of the hand-held smartphone (and thus the IMU) can vary in three dimensions. The dynamics of the IMU's attitude are modeled using a random walk in quaternion form given by

$$\frac{\mathrm{d}q_t^{\mathsf{I}}}{\mathrm{d}t} = \frac{1}{2} q_t^{\mathsf{I}} \odot \eta_{q,t}^{\mathsf{I}} \tag{3}$$

where q_t^{I} is the IMU's attitude quaternion relative to the persons coordinate frame, $\odot$ denotes the Hamiltonian product (quaternion multiplication), and $\eta_{q,t}$ is the driving white noise process with covariance S_q. Note that, depending on the interpretation of the stochastic differential equation (SDE) (3), different properties are obtained. If it is interpreted as an Îto-differential equation, the solution of the SDE might not preserve the norm constraint of the unit quaternion while the Stratonovich interpretation does not preserve the norm of the mean, see [12].

[1]Clearly, it is possible to account for the principal direction of motion in the global coordinate system by letting the process noise covariance depend on the direction of motion. However, the proposed approach here appears more intuitive.

B. Accelerometer Measurement Model

The measured acceleration consists of three components: 1) The person's acceleration a_t, 2) the gravitational acceleration g^{G}, and 3) oscillations caused by the quasi-periodic nature of the gait cycle, all rotated into the IMU coordinate frame.

The acceleration in the person's coordinate frame is found from the derivative of the velocity in the global coordinate frame v_t^{G} as follows

$$\begin{aligned} a_t^{\mathsf{G}} &= \frac{\mathrm{d}v_t^{\mathsf{G}}}{\mathrm{d}t} = \frac{\mathrm{d}}{\mathrm{d}t} v_t \begin{bmatrix} \cos(\psi_t) \\ \sin(\psi_t) \\ 0 \end{bmatrix} \\ &= a_t \begin{bmatrix} \cos(\psi_t) \\ \sin(\psi_t) \\ 0 \end{bmatrix} + v_t \omega_t \begin{bmatrix} -\sin(\psi_t) \\ \cos(\psi_t) \\ 0 \end{bmatrix} \\ &\approx v_t \omega_t \begin{bmatrix} -\sin(\psi_t) \\ \cos(\psi_t) \\ 0 \end{bmatrix} \end{aligned} \tag{4}$$

where it was assumed that the persons acceleration $a_t \approx 0$ most of the time. Then, rotating a_t^{G} into the person's coordinate frame yields

$$a_t^{\mathsf{P}} = R^{\mathsf{GP}} a_t^{\mathsf{G}} = \begin{bmatrix} 0 \\ v_t \omega_t \\ 0 \end{bmatrix}. \tag{5}$$

The inverse rotation matrix R^{GP} in (5) from the global reference G frame to the person's frame P is given by

$$R_t^{\mathsf{GP}} = \begin{bmatrix} \cos(\psi_t) & \sin(\psi_t) & 0 \\ -\sin(\psi_t) & \cos(\psi_t) & 0 \\ 0 & 0 & 1 \end{bmatrix}. \tag{6}$$

As indicated above, the swinging nature of the human gait causes quasi-periodic oscillations in the accelerometer measurement signal. In the person's reference frame, the longitudinal and vertical oscillations (in x- and z-direction, respectively) are mainly caused by the persons translation (forward gait), while the oscillations in the person's y-direction are caused by the rotation around the persons yaw-axis. One approach would be to model these oscillations directly in the measurement model using a Fourier series representation with unknown Fourier coefficients (two per harmonic). Another approach is to model the oscillations using stochastic resonators as in [13]. A stochastic resonator can be described by the following stochastic differential equation

$$\frac{\mathrm{d}}{\mathrm{d}t} \begin{bmatrix} \alpha_{n,t} \\ \dot{\alpha}_{n,t} \end{bmatrix} = \begin{bmatrix} 0 & \tilde{\omega}_n \\ -\tilde{\omega}_n & 0 \end{bmatrix} \begin{bmatrix} \alpha_t \\ \dot{\alpha}_t \end{bmatrix} + \begin{bmatrix} 0 \\ 1 \end{bmatrix} \eta_{\alpha,t}. \tag{7}$$

Thus, the observed pseudo-periodic oscillations in direction $i \in \{\mathsf{x}, \mathsf{y}, \mathsf{z}\}$ can be modeled as the sum of N_a^i stochastic resonators of the form (7)

$$a_{o,t}^{i,\mathsf{P}} = \sum_{n=1}^{N_a^i} \alpha_{n,t}^i \tag{8}$$

where N_a^i is the number of harmonics to include in the model (a tuning parameter). The frequency $\tilde{\omega}_n = 2\pi n f_0$ of the nth resonator has the fundamental frequency f_0 of half the step frequency

$$f_0 = \frac{|v_t|}{2l_s} \tag{9}$$

where l_s is the step length. Note that the step length l_s is generally unknown and varies from individual to individual (and possibly even from step to step).

Due to the finite truncation in (8) and unmodeled, possibly non-linear effects, the model does not explain the observed measurements entirely. Hence, a model uncertainty term $\epsilon_{a,t}^{\mathsf{P}}$ is added. $\epsilon_{a,t}^{\mathsf{P}}$ is parametrized in the person's coordinate frame such that it can account for the different degrees of confidence in the different models. As for the form of $\epsilon_{a,t}^{\mathsf{P}}$, we chose to represent it using a zero-mean Gaussian random variable with covariance $\Sigma_{\epsilon_{a,t}^{\mathsf{P}}}$, that is as

$$\epsilon_{a,t}^{\mathsf{P}} \sim \mathcal{N}(0, \Sigma_{\epsilon_{a,t}^{\mathsf{P}}}). \tag{10}$$

Finally, the complete accelerometer measurement model is obtained by collecting (5)-(10), adding the gravitational acceleration $g^{\mathsf{P}} = \begin{bmatrix} 0 & 0 & 9.81 \end{bmatrix}^\top$, rotating everything from the person's reference frame into the IMU coordinate frame and adding measurement noise. This yields

$$y_{a,t} = q_t^{\mathsf{I}*} \odot \left(g^{\mathsf{P}} + a_t^{\mathsf{P}} + a_{o,t}^{\mathsf{P}} + \epsilon_{a,t}^{\mathsf{P}} \right) \odot q_t^{\mathsf{I}} + n_{a,t} \tag{11}$$

where

$$a_{o,t}^{\mathsf{P}} = \begin{bmatrix} a_{o,t}^{\mathsf{x},\mathsf{P}} & a_{o,t}^{\mathsf{y},\mathsf{P}} & a_{o,t}^{\mathsf{z},\mathsf{P}} \end{bmatrix}^\top \tag{12}$$

and the measurement noise $n_{a,t}$ is assumed to be additive, white Gaussian noise of the form $n_{a,t} \sim \mathcal{N}(0, R_a)$.

C. Gyroscope Measurement Model

Similar to the accelerometer measurement model, the gyroscope measures the angular rate plus oscillations caused by the gait cycle. The angular rate (for the person) for in-plane motion is simply given by the yaw rate and zero pitch and roll rates, that is,

$$\omega_t^{\mathsf{P}} = \begin{bmatrix} 0 \\ 0 \\ \omega_t \end{bmatrix} \tag{13}$$

Furthermore, the predominant oscillating motion mainly manifests as yaw due to the body rotating around its z-axis while walking. Hence, we define a set of stochastic resonators analog to (7) as

$$\omega_{o,t}^{\mathsf{z},\mathsf{P}} = \sum_{n=1}^{N_\omega^{\mathsf{z}}} \beta_{n,t}^{\mathsf{z}} \tag{14}$$

and assume that

$$\omega_{o,t}^{\mathsf{x},\mathsf{P}} = \omega_{o,t}^{\mathsf{y},\mathsf{P}} \approx 0. \tag{15}$$

Again, the fundamental frequency is given by (9), $\beta_{n,t}^{\mathsf{z}}$ is the nth resonator, and N_ω^{z} is the number of resonators to be considered.

Additionally, an extra term $\epsilon_{\omega,t}^{\mathsf{P}} \sim \mathcal{N}(0, \Sigma_{\epsilon_{\omega,t}^{\mathsf{P}}})$ modeling the model uncertainties in the same way as in (10) is introduced. This finally yields the complete gyroscope measurement model

$$y_{\omega,t} = q_t^{\mathsf{I}*} \odot \left(\omega_t^{\mathsf{P}} + \omega_{o,t}^{\mathsf{P}} + \epsilon_{\omega,t}^{\mathsf{P}} \right) \odot q_t^{\mathsf{I}} + n_{\omega,t} \tag{16}$$

where $n_{a,t} \sim \mathcal{N}(0, R_\omega)$ is measurement noise, and $\omega_{o,t}^{\mathsf{P}} = \begin{bmatrix} 0 & 0 & \omega_{o,t}^{\mathsf{z},\mathsf{P}} \end{bmatrix}^\top$.

D. Magnetometer Measurement Model

The geomagnetic field is well studied and detailed models for different end purposes exist, see, for example [14]. In this work, a simple dipole model of the Earth's magnetic field is used. The magnitudes for the in-plane (x-y) and radial (z) magnetic fields are given by

$$B^{\mathsf{xy}} = B_0 \left(\frac{R_E}{r} \right)^3 \cos(\gamma) \tag{17a}$$

and

$$B^{\mathsf{z}} = -2B_0 \left(\frac{R_E}{r} \right)^3 \sin(\gamma), \tag{17b}$$

respectively. In (17), $B_0 = 31.2\,\mu\mathrm{T}$ is the magnetic field strength at the equator, $R_E = 6370\,\mathrm{km}$ the mean radius of the earth, r the radius at the person's location, and γ the magnetic latitude. Thus, the magnetic reference vector in the ENU coordinate frame is

$$B^{\mathsf{G}} = \begin{bmatrix} 0 \\ B^{\mathsf{xy}} \\ B^{\mathsf{z}} \end{bmatrix}. \tag{18}$$

Then, using (18) and the rotation matrix R^{GP} in (6), the magnetic field vector in the person's reference frame becomes

$$B_t^{\mathsf{P}} = R^{\mathsf{GP}} B^{\mathsf{G}} = \begin{bmatrix} B^{\mathsf{xy}} \sin(\psi_t) \\ B^{\mathsf{xy}} \cos(\psi_t) \\ B^{\mathsf{z}} \end{bmatrix}. \tag{19}$$

Additionally, since magnetometers most often suffer from a considerable bias [2], this bias b_m is modeled as a random walk

$$\frac{\mathrm{d}b_m}{\mathrm{d}t} = \eta_{b,t} \tag{20}$$

with $\eta_{b,t}$ a white noise process with covariance S_b.

Finally, the magnetometer measurement model is then given by

$$y_{m,t} = q_t^{\mathsf{I}} \odot B_t^{\mathsf{P}} \odot q_t^{\mathsf{I}} + b_m + n_{m,t} \tag{21}$$

where $n_{m,t} \sim \mathcal{N}(0, R_m)$ is the magnetometer measurement noise.

E. Discretization

In order to be able to implement the dynamic model, it has to be discretized. For the person's dynamic model (1), exact zero-order hold (ZOH) discretization yields [15]

$$\begin{bmatrix} p_k^{\mathsf{x}} \\ p_k^{\mathsf{y}} \\ v_k \\ \psi_k \\ \omega_k \end{bmatrix} = \begin{bmatrix} p_{k-1}^{\mathsf{x}} + \frac{2v_{k-1}\sin\left(\omega_{k-1}\frac{\Delta t}{2}\right)\cos\left(\psi_{k-1}+\omega_{k-1}\frac{\Delta t}{2}\right)}{\omega_{k-1}} \\ p_{k-1}^{\mathsf{y}} + \frac{2v_{k-1}\sin\left(\omega_{k-1}\frac{\Delta t}{2}\right)\sin\left(\psi_{k-1}+\omega_{k-1}\frac{\Delta t}{2}\right)}{\omega_{k-1}} \\ v_{k-1} \\ \psi_{k-1} + \omega_{k-1}\Delta t \\ \omega_{k-1} \end{bmatrix} + w_{v,k} \tag{22}$$

where k is the kth sampling instant and Δt is the time between the samples $k-1$ and k. The noise term $w_{v,k} \sim \mathcal{N}(0, Q)$ is assumed to be white Gaussian noise where a reasonable approximation of the covariance matrix Q can be obtained by first linearizing the system (1) and then using (31) (see Appendix).

Discretizing the IMU dynamics is more complex. A closed-form ZOH discretization of the quaternion dynamics for an arbitrary unit quaternion q with deterministic rotational velocity ω is given by

$$q_k = \Omega(\omega) q_{k-1}$$

with $\Omega(\omega)$

$$\Omega(w) = \cos\left(\|\omega\|\frac{\Delta t}{2}\right) I_4 + \begin{bmatrix} 0 & -[\omega]_1 & -[\omega]_2 & -[\omega]_3 \\ [\omega]_1 & 0 & [\omega]_3 & -[\omega]_2 \\ [\omega]_2 & -[\omega]_3 & 0 & [\omega]_1 \\ [\omega]_3 & [\omega]_2 & -[\omega]_1 & 0 \end{bmatrix} \frac{\sin\left(\|\omega\|\frac{\Delta t}{2}\right)}{\|\omega\|}$$

and $[\omega]_i$ denotes the ith component of the vector ω. However, since the IMU rotational velocity is modeled as a random variable, the above discretization does not strictly hold. Nevertheless, we found it to be a practical approximation and thus, the discretization for the IMU attitude is approximated as

$$q_k^{\mathsf{l}} = \Omega(w_{q,k}) q_{k-1}^{\mathsf{l}} \tag{23}$$

with $w_{q,k} \sim \mathcal{N}(0, Q_q)$ and an appropriate choice of Q_q.

Finally, the discretized equivalent of the stochastic resonator (7) is given by

$$\begin{bmatrix} \alpha_{n,k} \\ \dot{\alpha}_{n,k} \end{bmatrix} = \begin{bmatrix} \cos(\tilde{\omega}_n \Delta t) & \sin(\tilde{\omega}_n \Delta t) \\ -\sin(\tilde{\omega}_n \Delta t) & \cos(\tilde{\omega}_n \Delta t) \end{bmatrix} \begin{bmatrix} \alpha_{n,k-1} \\ \dot{\alpha}_{n,k-1} \end{bmatrix} + w_{\alpha_n,k} \tag{24}$$

where $w_{\alpha_n,k} \sim Q_{\alpha_n}$ is a white, Gaussian random variable with covariance Q_{α_n} (see again in the Appendix).

Summarizing the discretized dynamics in eqs. (22)-(24) and adding the measurement models (11), (16), and (21) finally yields the complete discretized state-space model which is of the form

$$x_k = f(x_{k-1}, w_{k-1}) \tag{25a}$$
$$y_k = g(x_k, n_k) \tag{25b}$$

with

$$x_k = \begin{bmatrix} p_k^{\mathsf{x}} & p_k^{\mathsf{y}} & v_k & \psi_k & \omega_k & q_k^{\mathsf{l}} & b_{m,k} & \tilde{\alpha}_k & \tilde{\beta}_k \end{bmatrix}^\top$$

where $\tilde{\alpha}_k$ is a vector containing all the pairs $\{\alpha_{n,k}^i, \dot{\alpha}_{n,k}^i\}\ \forall\, i \in \{\mathsf{x}, \mathsf{y}, \mathsf{z}\},\ n \in \{1, \ldots, N_a^i\}$ and similar for $\tilde{\beta}_k$. Furthermore,

$$y_k = \begin{bmatrix} y_{a,k} & y_{\omega,k} & y_{m,k} \end{bmatrix}^\top.$$

III. Estimation

The model derived in Section II can now readily be used for tracking. Note that since some states in both the state dynamics and observation functions are non-linear, a non-linear filter such as the extended or unscented Kalman filter (EKF/UKF), or a particle filter has to be used. Due to the large state dimension, an unscented Kalman filter is chosen. Note, however, that since the model has a linear substructure, a Rao-Blackwellized particle filter [16] would be equally well suited.

A. Norm-Constrained Unscented Kalman Filter

Even though it appears as if a standard unscented Kalman filter could be used directly, special care has to taken about the quaternion state q_k^{l}. Specifically, it has to be ensured that the unity of q_k^{l} is preserved. Thus, a norm-constrained Kalman filter where part of the state vector is subject to norm constraints is required [17], [18]. The algorithm is listed in Algorithm 1 where $x_k = \begin{bmatrix} x_k^u & x_k^c \end{bmatrix}^\top$ denotes the complete state vector, and x_k^u and x_k^c the unconstrained and constrained part of the state vector, respectively.

Algorithm 1 (Partially Norm-Constrained Unscented Kalman Filter)**.**

1) Set $\hat{x}_{0|0} = \mu_0$ and $P_{0|0} = \Sigma_0$, $k \leftarrow 1$.

2) Time update:

a) Calculate the sigma points:

$$\tilde{P} = \operatorname{blkdiag}(P_{k-1|k-1}, Q)$$
$$\delta x = \sqrt{(L+\lambda)\tilde{P}}$$
$$\mathcal{X}_{k-1|k-1} = \begin{bmatrix} \hat{x}_{k-1|k-1} & \hat{x}_{k-1|k-1} + \delta x & \hat{x}_{k-1|k-1} - \delta x \end{bmatrix}$$

b) Propagate the sigma points:

$$[\mathcal{X}_{k|k-1}]_{1:N_x,i} = f([\mathcal{X}_{k-1|k-1}]_{:,i}, [\mathcal{X}_{k-1|k-1}]_{N_x+1:L,i})$$

c) Predict the mean and covariance:

$$\hat{x}_{k|k-1} = \sum_{i=1}^{2L+1} [W_m]_i [\mathcal{X}_{k|k-1}]_{:,i}$$
$$P_{k|k-1} = \sum_{i=1}^{2L+1} [W_c]_i ([\mathcal{X}_{k|k-1}]_{:,i} - \hat{x}_{k|k-1}) \times ([\mathcal{X}_{k|k-1}]_{:,i} - \hat{x}_{k|k-1})^\top$$

3) Measurement update:

a) Calculate the sigma points:

$$\tilde{P} = \operatorname{blkdiag}(P_{k|k-1}, R)$$
$$\delta x = \sqrt{(L+\lambda)\tilde{P}}$$
$$\mathcal{X}_{k|k-1} = \begin{bmatrix} \hat{x}_{k|k-1} & \hat{x}_{k|k-1} + \delta x & \hat{x}_{k|k-1} - \delta x \end{bmatrix}$$

b) Predict the measurement:

$$[\mathcal{Y}_k]_i = g([\mathcal{X}_{k|k-1}]_{1:N_x,i}, [\mathcal{X}_{k|k-1}]_{N_x+1:M,i})$$

c) Calculate the innovation and covariances:

$$\begin{aligned}\hat{y}_k &= \sum_{i=1}^{2M+1} [W_m]_i [\mathcal{Y}_k]_i \\ C_{xy} &= \sum_{i=1}^{2M+1} [W_c]_i ([\mathcal{X}_{k|k-1}]_{1:N_x,i} - \hat{x}_{k|k-1}) \\ &\qquad \times ([\mathcal{Y}_k]_i - \hat{y}_k)^\top \\ C_{yy} &= \sum_{i=1}^{2M+1} [W_c]_i ([\mathcal{Y}_k]_i - \hat{y}_k)([\mathcal{Y}_k]_i - \hat{y}_k)^\top\end{aligned}$$

d) Update the mean and covariance:

$$\begin{aligned}K_k &= C_{xy} C_{yy}^{-1} \\ \hat{x}_{k|k} &= \hat{x}_{k|k-1} + K_k(y_k - \hat{y}_k) \\ P_{k|k} &= P_{k|k-1} - K_k C_{yy} K_k^\top\end{aligned}$$

4) Normalization:

$$\hat{x}^c_{k|k} = \frac{\sqrt{l}}{\|\hat{x}^c_{k|k}\|} \hat{x}^c_{k|k}$$

5) Set $k \leftarrow k+1$ and return to step 2. □

In Algorithm 1, $L = N_x + N_w$ is the dimension of the augmented state in the time update and similarly, $M = N_x + N_n$ is the dimension of the augmented state in the measurement update. Furthermore,

$$[W_m]_i = \begin{cases} \frac{\lambda}{L+\lambda} & i = 1 \\ \frac{1}{2(L+\lambda)} & i = 2, \ldots, 2L+1 \end{cases}$$

and

$$[W_c]_i = \begin{cases} \frac{\lambda}{L+\lambda} + (1 - \alpha^2 + \beta) & i = 1 \\ \frac{1}{2(L+\lambda)} & i = 2, \ldots, 2L+1 \end{cases}$$

are the mean and covariance weights, respectively. α, β, and κ are filter parameters and

$$\lambda = \alpha^2(L + \kappa) - L.$$

Finally, the notation $[A]_{i,j}$ refers to the i-th row, j-th column entry of the matrix A where a semicolon indicates the whole column (or row).

Note that the only difference between the regular unscented Kalman filter and its norm-constrained version is step 4 where the normalization is performed: The constrained states $\hat{x}^c_{k|k}$ can simply normalized after a regular filter update (as it has been shown that this is equivalent to calculating a constrained filter gain, see [17], [18]).

B. Initialization

In order to get good performance, good initialization with proper initial state estimates μ_0 is crucial. Thus, strategies for initializing the state in an appropriate manner are presented below, where $\bar{y}$ denotes a batch of initialization data.

1) Position: If some sort of global position information is available, for example from satellite positioning systems or Bluetooth beacons, this position information can be used to initialize the position. Otherwise, nothing can be said about the global position and it is assumed that $p_0^{\mathsf{x}} = p_0^{\mathsf{y}} = 0$.

2) IMU Attitude: The initial IMU attitude can be estimated based on the initial accelerometer measurements while static (i.e. based on the local gravity vector). The pitch and roll angles of the IMU are then given by

$$\theta_0^{\mathsf{I}} = \operatorname{atan2}(\bar{y}_a^{\mathsf{y}}, \bar{y}_a^{\mathsf{z}}) \tag{26a}$$

and

$$\varphi_0^{\mathsf{I}} = \operatorname{atan2}\left(-\bar{y}_a^{\mathsf{x}}, \sqrt{(\bar{y}_a^{\mathsf{y}})^2 + (\bar{y}_a^{\mathsf{z}})^2}\right), \tag{26b}$$

respectively. Additionally, the initial yaw ψ_0^{I} with respect to the user has to be determined. This is not trivial as it is well known that the yaw angle is unobservable from gravity measurements only. Instead, we can initialize the yaw angle based on the (presumed) orientation of the device.

$$\psi_0^{\mathsf{I}} = \begin{cases} 0 & \text{Landscape} \\ -\pi & \text{Landscape, upside down} \\ -\pi/2 & \text{Portrait} \\ \pi/2 & \text{Portrait, upside down} \end{cases} \tag{26c}$$

Once all three Euler angles are determined, these can be converted to the initial attitude quaterinion q_0^{I} using the well-known conversion rule, see [19].

3) Heading, Magnetic Latitude, and Bias: Once the IMU attitude is determined, the heading can be estimated from the initial (calibrated) magnetometer measurements as follows. First, the initialization data is transformed to the person's reference frame as $\tilde{y}_m = R^{\mathsf{IP}} \bar{y}_m$ and then the heading is found as

$$\psi_0 = \operatorname{atan2}(\tilde{y}_m^{\mathsf{x}}, \tilde{y}_m^{\mathsf{y}}). \tag{27}$$

Furthermore, the magnetic latitude can be estimated from the magnitude of the magnetic measurements. Using (17), the magnitude is found to be

$$\begin{aligned}\|B\| &= \sqrt{B^{\mathsf{xy}2} + B^{\mathsf{z}2}} \\ &= B_0 \left(\frac{R_E}{r}\right)^3 \sqrt{\cos^2(\gamma) + 4\sin^2(\gamma)} \\ &= B_0 \left(\frac{R_E}{r}\right)^3 \sqrt{1 + 3\sin^2(\gamma)}\end{aligned}$$

where the identity $\cos^2(\gamma) = 1 - \sin^2(\gamma)$ was used in the last step. Solving for γ and replacing the magnitude $\|B\|$ with the observed magnitude $\|\bar{y}_m\|$ thus yields

$$\gamma = \operatorname{asin}\left(\frac{1}{\sqrt{3}}\left(\left(\frac{\|\bar{y}_m\|}{B_0}\left(\frac{r}{R_E}\right)^3\right)^2 - 1\right)^{1/2}\right). \tag{28}$$

Finally, an initial estimate of the magnetometer bias can then be found as

$$b_m = \bar{y}_m - R^{\mathsf{pl}} \begin{bmatrix} B^{\mathsf{xy}} \sin(\psi_0) \\ B^{\mathsf{xy}} \cos(\psi_0) \\ B^{\mathsf{z}} \end{bmatrix}. \tag{29}$$

4) Remaining States: Since no measurements of the remaining states (velocity, angular velocity, and the stochastic resonators) are available, these states are simply initialized as being zero.

IV. Experimental Results

In this section, the proposed method is evaluated using real experiments. The experiment setup is described next, followed by the results and their evaluation.

A. Experimental Setup

The experimental setup was as follows. A test subject was instructed to normally walk a predefined trajectory, keeping an LG Nexus 5 smartphone casually in the hand. The data from the device's IMU (InvenSense MPU6515) and magnetometer (AKM AK8963) were then recorded on the device. The sampling rates were chosen to the highest possible rates which were 200 Hz for the IMU and 50 Hz for the magnetometer. In addition to the IMU and magnetometer data, the walked trajectory was recorded using the built-in Global Positioning System receiver in order to obtain a reference trajectory. The data were then processed off-line with the model and UKF as described in Sections II-III implemented in Matlab.

B. Results

Fig. 2 shows the estimated trajectory together with the GPS reference path. As it can be seen, the proposed method manages to capture the overall shape of the trajectory but suffers from some heading issues. This is especially prominent in the second half of the trajectory (after the second turn) where there is a slight bend causing the trajectory to diverge. However, even after that bend, the trajectory retains the overall true shape but is slightly rotated, suggesting a bias in the heading from that point on. Furthermore, the total length of the reference trajectory (GPS) is 302 m whereas the total length estimated by the proposed method is 293 m.

The states for translation and orientation are shown in Figs. 3 and 4, respectively. Figs. 3a and 3b show the estimated x-y-coordinates together with the GPS reference. A first observation is that the estimated curve appears to start somewhat later, indicating that it takes some time for the filter to transition from standing still to moving. Closer inspection revealed that this delay is about 5 s which, at a speed of 1.5 m/s, corresponds to 7.5 m. Hence, this could be one possible explanation for the difference in length to the turn of the two trajectories (see bottom right corner in Fig. 2). Furthermore, the slope of the first half of the GPS as well as the estimated are roughly parallel, indicating that the speed estimate, which averages around 1.5 m/s (c.a. 5.4 km/h) (Fig. 3c), is reasonable.

[3]Map data © OpenStreetMap contributors, see http://www.openstreetmap.org/copyright.

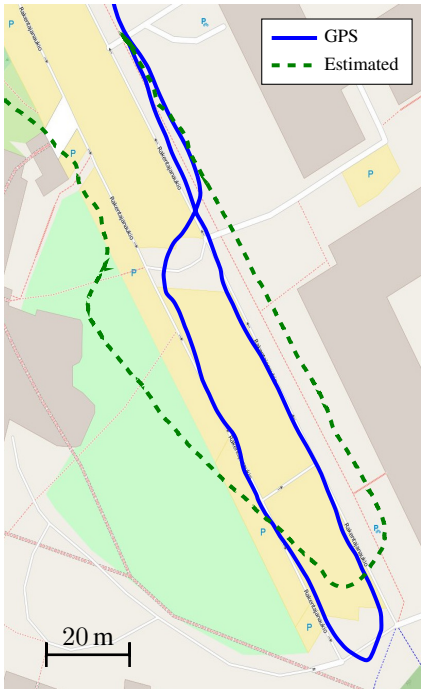

Fig. 2. Estimated trajectory (green, dashed) together with the GPS reference path (blue, solid), overlaid onto the local map[3].

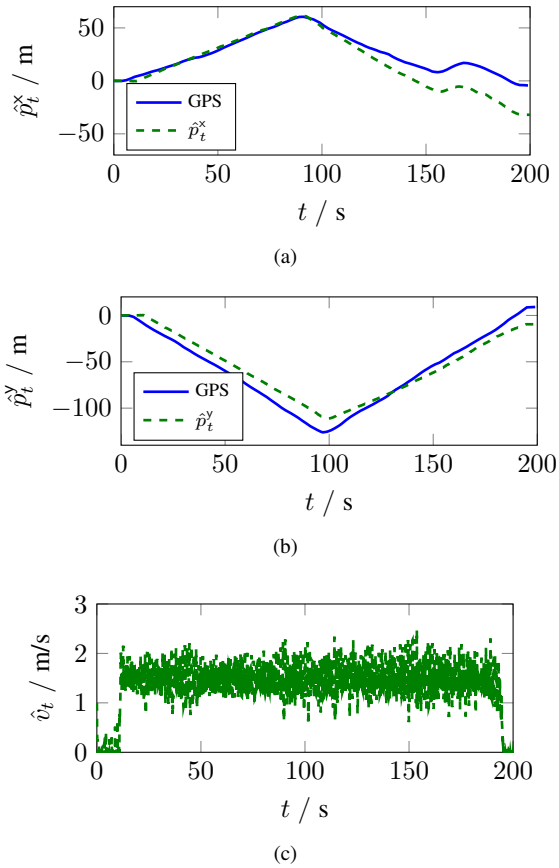

Fig. 3. Position- and speed estimates. (a) x-position, (b) y-position, and (c) speed.

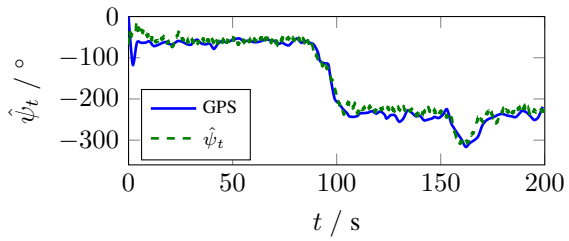

(a)

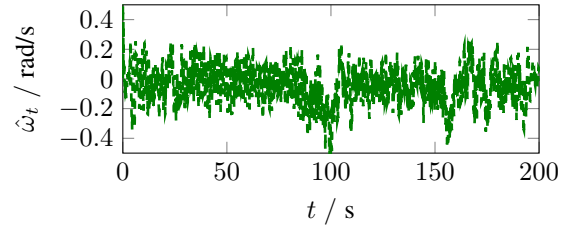

(b)

Fig. 4. Estimated orientation. (a) Heading and (b) rotational velocity.

Similarly, Fig. 4a shows the estimated heading together with the reference heading calculated by the GPS position differences. As it can be seen, the headings closely follow each other in the beginning. After $t \approx 100\,\mathrm{s}$, however, the proposed method's heading is somewhat larger than the GPS' heading which again corresponds to the divergence observed in Fig. 2.

C. Discussion

The results indicate that the method is feasible. The main problems observed were a dead-time upon start and a slight heading drift after a while. The delayed start issue might be addressed by fine-tuning the filter's parameters or by extending the method to use an interacting multiple model approach with modes for stationarity as well as motion. The heading drift problem could be mitigated by using a more sophisticated geomagnetic field model (as it is known that the dipole model is fairly crude) and taking temporary disturbances such as bypassing cars or other structures into account. Another aspect is the fact that the step length has been assumed fixed and known. As it has been shown in the literature (see, for example [11], [20]), this should rather be estimated either from a person's physical attributes or directly from the measurement data (which would require some extensions to the measurement model).

Furthermore, in the performed experiments, the phone was held in a fairly constant position. While the model is derived to work with arbitrary orientation and placement, the assumption of negligible acceleration of the phone itself should not be violated. Hence, an open question is also how sensitive the method is to other placements (e.g. back pocket, handbag, etc.) and dynamic situations where the phone is moved between different orientations and placements.

The proposed method could easily be extended to make use of map matching. This would help stabilizing the heading estimate and would also address scaling issues. Finally, a norm-constrained unscented Kalman filter was used for estimating the trajectory. Clearly, more advanced filtering techniques such as particle filters or the recently developed filters for heavy-tailed noise [21] have the potential to improve the accuracy and robustness of the overall PDR system.

V. Conclusions

In this paper, complete motion- and observation models for IMU and magnetometer-based pedestrian dead-reckoning that neither rely on step detection nor zero-velocity updates have been developed. The experimental results show that the proposed approach is feasible and possible limitations and extensions have been pointed out.

Future work will include more tests with arbitrary positioning of the phone, for example in pockets or handbags, in order to test the robustness toward these variations. Furthermore, the issues encountered in the experimental evaluation – heading drift and somewhat long convergence time – need further investigation.

Appendix

Given the linear dynamic SDE

$$\frac{\mathrm{d}x}{\mathrm{d}t} = Ax + B\eta$$

with the zero-mean, white random process η with covariance S, ZOH discretization yields

$$x_k = \Gamma x_{k-1} + w_k$$

where $w_k \sim \mathcal{N}(0, Q)$,

$$\Gamma = \exp(A\Delta t), \tag{30}$$

$$Q = \int_0^{\Delta t} \exp(A(\Delta t - \tau))BSB^\top \exp(A(\Delta t - \tau))^\top \mathrm{d}\tau, \tag{31}$$

and $\exp(At)$ is the matrix exponential which can, for example, be calculated using the Laplace transform.

Then, the discretized motion model's covariance is found from linearizing the continuous time model and then discretizing it using (30)-(31). It is given by

$$Q = \begin{bmatrix} Q_T & Q_{TR} \\ Q_{TR}^\top & Q_R \end{bmatrix} \tag{32}$$

where

$$Q_T = S_v \begin{bmatrix} \frac{\Delta t^3 \cos^2(\psi)}{3} & \frac{\Delta t^3 \cos(\psi)\sin(\psi)}{3} & \frac{\Delta t^2 \cos(\psi)}{2} \\ \frac{\Delta t^3 \cos(\psi)\sin(\psi)}{3} & \frac{\Delta t^3 \sin^2(\psi)}{3} & \frac{\Delta t^2 \sin(\psi)}{2} \\ \frac{\Delta t^2 \cos(\psi)}{2} & \frac{\Delta t^2 \sin(\psi)}{2} & \Delta t \end{bmatrix} + S_r \frac{v^2 \Delta t^5}{20} \begin{bmatrix} \sin^2(\psi) & -\cos(\psi)\sin(\psi) & 0 \\ -\cos(\psi)\sin(\psi) & \cos^2(\psi) & 0 \\ 0 & 0 & 0 \end{bmatrix}$$

$$Q_{TR} = S_r v \begin{bmatrix} -\frac{\Delta t^4 \sin(\psi)}{8} & -\frac{\Delta t^3 \sin(\psi)}{6} \\ \frac{\Delta t^4 \cos(\psi)}{8} & \frac{\Delta t^3 \cos(\psi)}{6} \\ 0 & 0 \end{bmatrix}$$

$$Q_R = S_r \begin{bmatrix} \frac{\Delta t^3}{3} & \frac{\Delta t^2}{2} \\ \frac{\Delta t^2}{2} & \Delta t \end{bmatrix}$$

For the stochastic resonators, no linearization is necessary. Hence, (30)-(31) can be used directly and the stochastic resonators' covariance matrix becomes

$$Q_{\alpha_n} = \frac{S_{\alpha_n}}{2\tilde{\omega}_n} \begin{bmatrix} \tilde{\omega}_n \Delta t - \sin(2\tilde{\omega}_n \Delta t) & \sin^2(\tilde{\omega}_n \Delta t) \\ \sin^2(\tilde{\omega}_n \Delta t) & \tilde{\omega}_n \Delta t + \sin(2\tilde{\omega}_n \Delta t) \end{bmatrix}.$$

ACKNOWLEDGMENT

Financial support by the Academy of Finland under the grant no. #295080 (CrowdSLAM) is hereby gratefully acknowledged.

REFERENCES

[1] C. Fischer and H. Gellersen, "Location and navigation support for emergency responders: A survey," *IEEE Pervasive Computing*, vol. 9, no. 1, pp. 38–47, January 2010.

[2] D. Titterton and J. Weston, *Strapdown Inertial Navigation Technology*, 2nd ed. The Institution of Engineering and Technology, 2004.

[3] E. Foxlin, "Pedestrian tracking with shoe-mounted inertial sensors," *IEEE Computer Graphics and Applications*, vol. 25, no. 6, pp. 38–46, November 2005.

[4] J.-O. Nilsson, A. K. Gupta, and P. Händel, "Foot-mounted inertial navigation made easy," in *Indoor Positioning and Indoor Navigation (IPIN), 2014 International Conference on*, October 2014, pp. 24–29.

[5] F. Zampella, M. Khider, P. Robertson, and A. Jiménez, "Unscented Kalman filter and magnetic angular rate update (maru) for an improved pedestrian dead-reckoning," in *Position Location and Navigation Symposium (PLANS), 2012 IEEE/ION*, April 2012, pp. 129–139.

[6] R. Harle, "A survey of indoor inertial positioning systems for pedestrians," *IEEE Communications Surveys Tutorials*, vol. 15, no. 3, pp. 1281–1293, 2013.

[7] W. Kang and Y. Han, "SmartPDR: smartphone-based pedestrian dead reckoning for indoor localization," *IEEE Sensors Journal*, vol. 15, no. 5, pp. 2906–2916, May 2015.

[8] T. Do-Xuan, V. Tran-Quang, T. Bui-Xuan, and V. Vu-Thanh, "Smartphone-based pedestrian dead reckoning and orientation as an indoor positioning system," in *2014 International Conference on Advanced Technologies for Communications (ATC 2014)*, October 2014, pp. 303–308.

[9] M. Susi, V. Renaudin, and G. Lachapelle, "Motion mode recognition and step detection algorithms for mobile phone users," *Sensors*, vol. 13, no. 2, pp. 1539–1562, 2013.

[10] C. Randell, C. Djiallis, and H. Muller, "Personal position measurement using dead reckoning," in *Wearable Computers, 2003. Proceedings. Seventh IEEE International Symposium on*, October 2003, pp. 166–173.

[11] Z. Xiao, H. Wen, A. Markham, and N. Trigoni, "Robust pedestrian dead reckoning (R-PDR) for arbitrary mobile device placement," in *Indoor Positioning and Indoor Navigation (IPIN), 2014 International Conference on*, October 2014, pp. 187–196.

[12] B. Øksendal, *Stochastic Differential Equaitons: An Introduction with Applications*, 6th ed. Springer, 2010.

[13] S. Särkkä, A. Solin, A. Nummenmaa, A. Vehtari, T. Auranen, S. Vanni, and F.-H. Lin, "Dynamic retrospective filtering of physiological noise in BOLD fMRI: DRIFTER," *NeuroImage*, vol. 60, no. 2, pp. 1517 – 1527, 2012.

[14] G. Backus, R. Parker, and C. Constable, *Foundations of Geomagnetism*. Cambridge University Press, 2005.

[15] X. R. Li and V. P. Jilkov, "Survey of maneuvering target tracking. Part I. Dynamic models," *IEEE Transactions on Aerospace and Electronic Systems*, vol. 39, no. 4, pp. 1333–1364, October 2003.

[16] T. B. Schön, F. Gustafsson, and P.-J. Nordlund, "Marginalized particle filters for mixed linear/nonlinear state-space models," *IEEE Transactions on Signal Processing*, vol. 53, no. 7, pp. 2279–2289, July 2005.

[17] R. Zanetti, M. Majji, R. H. Bishop, and D. Mortari, "Norm-constrained Kalman filtering," *Journal of Guidance, Control, and Dynamics*, vol. 32, no. 5, pp. 1458–1465, 2009.

[18] D. Simon, "Kalman filtering with state constraints: a survey of linear and nonlinear algorithms," *IET Control Theory Applications*, vol. 4, no. 8, pp. 1303–1318, August 2010.

[19] J. Diebel, "Representing attitude: Euler angles, unit quaternions, and rotation vectors," Stanford University, Tech. Rep., 2006.

[20] V. Renaudin, M. Susi, and G. Lachapelle, "Step length estimation using handheld inertial sensors," *Sensors*, vol. 12, no. 7, p. 8507, 2012.

[21] F. Tronarp, R. Hostettler, and S. Särkkä, "Sigma-point filtering for nonlinear systems with non-additive heavy-tailed noise," in *The 19th International Conference on Information Fusion (FUSION)*, Heidelberg, Germany, July 2016.